PAPER

Check for updates

A new dithieno[3,2-b:2′,3′-d]thiophene derivative for high performance single crystal organic field-effect transistors and UV-sensitive phototransistors†

Yunpeng Lou,[a] Rui Shi,[a] Li Yu,[a] Ting Jiang,[a] Haoquan Zhang,[a] Lifeng Zhang,[d] Yongxu Hu,[a] Deyang Ji, [iD][a] Yajing Sun,*[b] Jie Li, [iD]*[a] Liqiang Li [iD][ac] and Wenping Hu[bc]

Organic phototransistors (OPTs), as the basic unit for organic image sensors, are emerging as one of the most promising light signal detectors. High performance UV-sensitive phototransistors are highly desired for the detection of UV light. Herein, by introducing the anthracene group to the 2,6-positions of dithieno[3,2-b:2′,3′-d]thiophene, we designed and synthesized a new dithieno[3,2-b:2′,3′-d]thiophene derivative, 2,6-di(anthracen-2-yl)dithieno[3,2-b:2′,3′-d]thiophene (2,6-DADTT). The single crystal structure of 2,6-DADTT presents classical herringbone packing with multiple intermolecular interactions, including S···S (3.470 Å), S···C (3.304 Å, 3.391 Å, 3.394 Å) and C−H···π (2.763 Å, 2.822 Å, 2.846 Å, 2.865 Å, 2.885 Å, 2.890 Å) contacts. Single crystal organic field-effect transistors (SC-OFETs) based on 2,6-DADTT reach a highest mobility of 1.26 cm^2 V^{-1} s^{-1} and an average mobility of 0.706 cm^2 V^{-1} s^{-1}. 2,6-DADTT-based single crystal organic phototransistors (OPTs) demonstrate photosensitivity (P) of 2.49 × 10^6, photoresponsivity (R) of 6.84 × 10^3 A W^{-1} and ultrahigh detectivity (D^*) of 4.70 × 10^{16} Jones to UV light, which are among the best figures of merit for UV-sensitive OPTs. These excellent comprehensive performances indicate its good application prospects in integrated optoelectronics.

Introduction

In recent decades, organic semiconductors (OSCs) have attracted intensive attention due to their advantages such as diverse functional modification,[1–3] light weight, intrinsic flexibility,[4–8] easy large-area solution processing,[9–12] and better compatibility with a flexible substrate or biosystem,[13,14] and have found applications in many fields, including organic field-effect transistors (OFETs),[15–20] organic light-emitting transistors (OLETs),[21–27] organic light-emitting diodes (OLEDs),[28–30] organic photovoltaics (OPVs),[31–33] organic photo detectors (OPDs)[34–38] and so on.

Organic phototransistors (OPTs), as the basic unit for organic image sensors, are emerging as one of the most promising light signal detectors owing to the unique advantages of OSCs mentioned above. Generally, the working mechanism of OPTs is as follows: organic semiconductors absorb photons and generate excitons; the photo-generated excitons in OSCs undergo exciton diffusion and dissociate into free charge carriers; the free charge carriers flow to corresponding electrodes and lead to the change of current signal.[39] Thanks to the joint efforts of researchers in the fields of chemistry, materials, physics, electronics, *etc.*, OPTs have witnessed remarkable achievements recent years. The key figures of merits of some OPTs are now comparable or even higher than those of silicon-based or inorganic phototransistors.[36,40–46] In spite of the exciting results, there are still problems remained to be solved in this field. For example, UV-detection is highly desired due to its important application in the fields of defence, information communications and biomedicine, while UV-sensitive OPTs are rarely studied due to the multiple requirements for organic semiconductors (high mobility, unique absorption in the UV region). Till now, only a few UV-sensitive OPTs with comprehensive high performances are reported. Hu *et al.* reported a kind of benzo[1,2-b:4,5-b′]dithiophene dimers linked with double bonds, (E)-1,2-bis(benzo[1,2-b:4,5-b′]dithiophen-2-yl) ethene (BBDTE), and the single crystal phototransistors based on which show photosensitivity of 10^5 and high photo-responsivity of 9821 A W^{-1} under the 380 nm UV light.[42] Meng

[a]Tianjin Key Laboratory of Molecular Optoelectronic Sciences, Department of Chemistry, Institute of Molecular Aggregation Science, Tianjin University, Tianjin 300072, China. E-mail: syg19@tju.edu.cn; lijie2018@tju.edu.cn

[b]Tianjin Key Laboratory of Molecular Optoelectronic Sciences, Department of Chemistry, School of Science, Tianjin University, Tianjin 300072, China

[c]Joint School of National University of Singapore and Tianjin University, International Campus of Tianjin University, Binhai New City, Fuzhou 350207, China

[d]Institute of Molecular Plus, Tianjin University, Tianjin 300072, China

et al. reported a kind of anthracene derivatives, 2,6-bis(4-methoxyphenyl) anthracene (BOPAnt), which exhibits a photosensitivity of 2×10^5, and a photoresponsivity of 3100 A W^{-1} upon illumination of 350 nm UV light with intensity of 0.11 mW cm^{-2}.[43] Tian *et al.* reported a novel pyrene derivative containing large steric hindrance triphenylamine groups and being linked by triple bonds, and the corresponding single crystal phototransistors exhibit excellent performance with photosensitivity of 1.60×10^5 photoresponsivity of 2.86×10^6 A W^{-1} and ultrahigh detectivity of 1.49×10^{18} Jones under 370 nm light irradiation.[44] Overall speaking, it is still highly demanded to develop high mobility organic semiconductors with unique absorption in the UV region to achieve high performance UV-sensitive OPTs and to further study the structure–property relationship.

Herein, we synthesized a new compound 2,6-di(anthracen-2-yl)dithieno[3,2-*b*:2′,3′-*d*]thiophene (2,6-DADTT) by linking 2,6-[3,2-*b*:2′,3′-*d*]thiophene (*tt*-DTT) with anthracene group with the following considerations: (i) the collaboration of S⋯S interaction, π–π or C–H⋯π interactions of sulfur-rich organic semiconductors may offer more charge transport pathways, leading to enhanced transport properties;[47,48] (ii) the introduction of anthracene moiety is expected for aromatic extension to offer more efficient π orbital overlap. Single crystal structure shows that 2,6-DADTT molecules pack in a classical herringbone packing motif with multiple S⋯S interactions, S⋯C interactions and C–H⋯π interactions. Single crystal organic field-effect transistors (SC-OFETs) based on 2,6-DADTT demonstrate excellent electrical properties, with the highest mobility of 1.26 cm^2 V^{-1} s^{-1} and high current on/off ratio of $10^6 \sim 10^8$. The single crystal OPTs of 2,6-DADTT also exhibit superb performance with excellent photosensitivity (*P*) of 2.49×10^6, photoresponsivity (*R*) of 6.84×10^3 A W^{-1} and ultrahigh detectivity (*D**) of 4.70×10^{16} Jones upon weak 365 nm UV light illumination with intensity of 0.024 mW cm^{-2}.

Results and discussion

2,6-DADTT was facilely synthesized by one step Suzuki coupling, as illustrated in Scheme 1, and then purified by vacuum sublimation for three times before further device fabrication. For the solubility of the 2,6-DADTT, it is only slightly soluble in common organic solvents. The UV-visible absorption spectra of 2,6-DADTT were shown in Fig. 1a. Both 2,6-DADTT film and crystals demonstrated obvious red-shifted absorption (∼20 nm) when comparing with the absorption in solution, suggesting that 2,6-DADTT molecules adopted J-aggregated mode in the aggregated state. The fluorescence spectra of 2,6-DADTT were shown in Fig. 1b. 2,6-DADTT crystals showed bright orange emission (Fig. S1†) under UV light
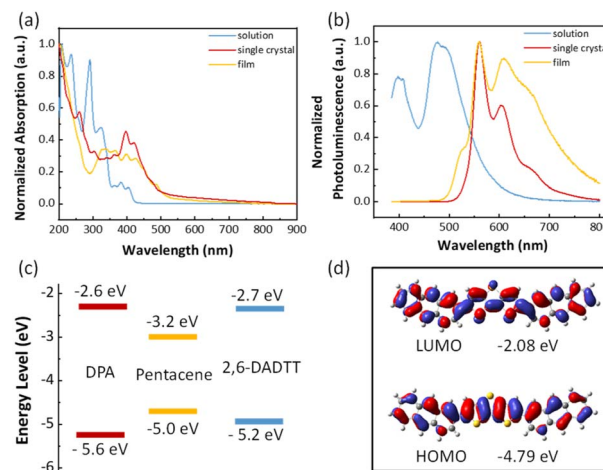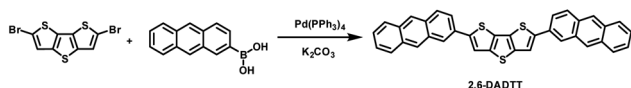

Fig. 1 (a) Normalized UV-vis spectra of 2,6-DADTT. (b) Normalized photoluminescence spectra of 2,6-DADTT. (c) Energy levels of 2,6-DADTT and referenced semiconductors. (d) The LUMO and HOMO energy levels of 2,6-DADTT calculated by density functional theory (DFT).

irradiation with main emission peaks located at 560 nm, 604 nm respectively. The photophysical properties of 2,6-DADTT, including absorption and emission parameters, were listed in Fig. S2 and Table S1.† The highest occupied molecular orbital (HOMO) energy level, calculated from ultraviolet photoelectron spectroscopy (UPS, Fig. S3†) was −5.2 eV. According to the empirical formula $E_g = 1240/\lambda$, the optical bandgap (E_g^{opt}) estimated from the onset of the thin film absorption is 2.5 eV, so the lowest unoccupied orbital energy (LUMO) level was calculated to be −2.7 eV, correspondingly. The energy levels were aligned in Fig. 1c, with 2,6-DPA and pentacene as references. The LUMO and HOMO energy levels were also calculated by density functional theory (DFT), showing that the π–electrons distribute uniformly over the whole molecule (Fig. 1d). Thermo gravimetric analysis (TGA, Fig. S4†) shows that the corresponding temperature at 5% weight loss of 2,6-DADTT is 471 °C, which indicates its excellent thermal stability.

The large-sized 2,6-DADTT single crystals qualified for X-ray diffraction analysis were prepared by physical vapor transport method. The single crystal structure of 2,6-DADTT belongs to the $P2_1/c$ space group with the lattice constants $a = 7.4830(3)$ Å, $b = 5.9649(2)$ Å, $c = 55.0355(14)$ Å, $\beta = 101.485(3)°$ (CCDC: 2237416, Table S2 and Fig. S5†). As shown in Fig. 2a, the torsion angles between dithieno[3,2-*b*:2′,3′-*d*]thiophene core and the anthracene group are 0.83° and 0.97°, respectively, showing excellent coplanarity property and effective aromatic extension. The 2,6-DADTT molecules stack in a classical herringbone packing motif with a herringbone angle of 43.00° (Fig. 2b). Multiple intermolecular interactions between the neighbouring molecules are observed for 2,6-DADTT molecules, including S⋯S (3.470 Å), S⋯C (3.304 Å, 3.391 Å, 3.394 Å) and C–H⋯π (2.763 Å, 2.822 Å, 2.846 Å, 2.865 Å, 2.885 Å, 2.890 Å) contacts (Fig. 2c). These short contacts between molecules together with the intramolecular S⋯H interaction (2.589 Å, 2.584 Å, Fig. S6†) lock the anthracene group and the dithieno[3,2-*b*:2′,3′-*d*]

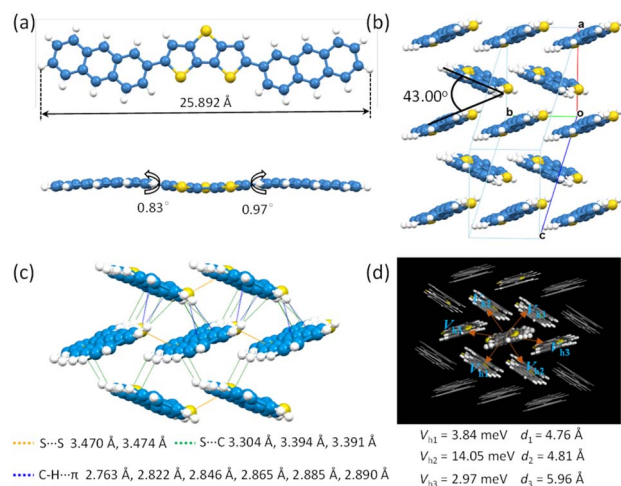**Scheme 1** Synthetic route to 2,6-DADTT.

Fig. 2 (a)–(c) Single crystal structures and (d) calculated transfer integrals of 2,6-DADTT.

thiophene core, which lead to small torsion angles between the anthracene group and the dithieno[3,2-*b*:2′,3′-*d*]thiophene core and excellent planar structure of 2,6-DADTT, while these interactions such as S···S contacts and C–H···π contacts greatly improve the closely packing, which is conducive to charge transport between molecules. The molecular integrals were also calculated based on the single crystal structure of 2,6-DADTT (Fig. 2d), showing multiple charge transfer pathways with transfer integrals of 14.05 meV, 3.84 meV, 2.97 meV.

Organic single crystals are believed to be an excellent platform to investigate the intrinsic optoelectronic property of organic semiconductors because of their highly ordered molecular packing and reduced grain boundaries. Micro-sized 2,6-DADTT crystals suitable for device fabrication were firstly produced by PVT method. Optical microscopy, atomic force microscopy (AFM), X-ray diffraction (XRD), and transmission electron microscope (TEM) were used to characterize the morphology and molecular packing structure of the 2,6-DADTT single crystals on substrate. As shown in Fig. 3a, the 2,6-DADTT
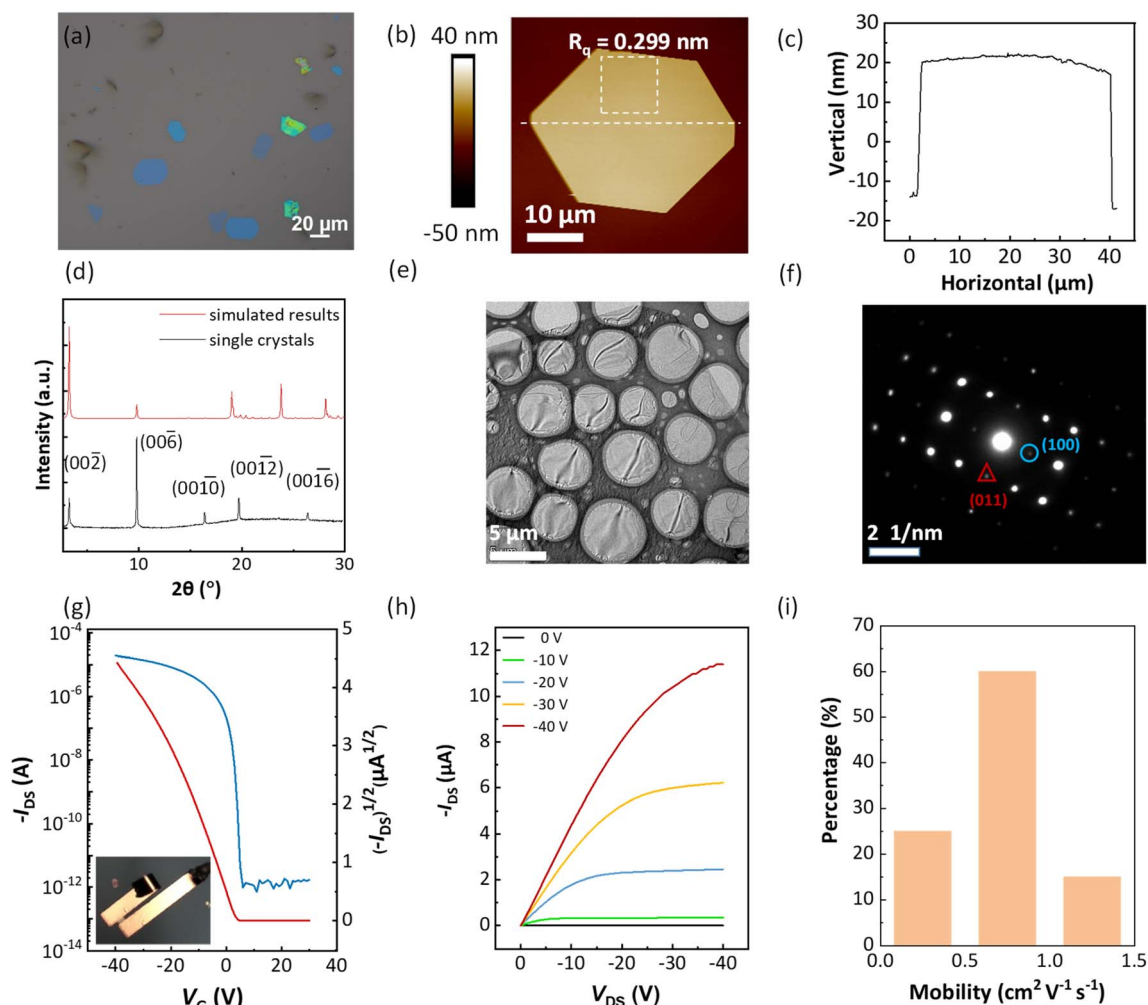

Fig. 3 (a) Optical microscopy of the single crystals prepared by PVT method. (b) Atomic force microscopy of an individual single crystal and its corresponding height profile (c). (d) XRD of 2,6-DADTT single crystals with the simulated results according to the single crystal structure for reference. (e) TEM of an individual 2,6-DADTT single crystal and its corresponding SAED result (f). (g) Typical transfer curve (inset: optical microscopy of the device) and corresponding output curve (h) of the 2,6-DADTT-based SC-OFETs. (i) Mobility distribution of twenty 2,6-DADTT-based SC-OFET devices.

single crystals grow plate-like with sizes ranging from several micrometres to tens of micrometres. The polarized optical microscope (POM) of an individual single crystal presented in Fig. S7† also shows obvious brightness change when rotating the sample, suggesting the high crystallinity of the 2,6-DADTT single crystal. As show in Fig. 3b and c, the AFM image indicates that the single crystal of 2,6-DADTT on wafer has a quite smooth surface with the root mean square roughness (R_q) value of about 0.299 nm and the height is 30 nm approximately. The sharp diffraction peaks can be well assigned to $(00l)$ according to the single crystal structure, suggesting that the ab-plane is paralleled to the substrate and the layer-by-layer growth mode of the 2,6-DADTT molecules on the wafer. The d-spacing calculated from the first order of the diffraction peak $(2\theta = 3.27°)$ is 26.97 Å, corresponds with the molecular length of 2,6-DADTT (25.892 Å). The TEM image of an individual single crystal and its corresponding selected area electron diffraction (SAED) patterns were shown in Fig. 3e and f. The bright diffraction pattern indicates the high quality of the 2,6-DADTT single crystal and the direction can be defined as (011) and (100). The bottom-gate-top-contact single crystal organic field-effect transistors (SC-OFETs) were then constructed by laminating the gold source/drain electrode on the micro-sized 2,6-DADTT single crystal using "gold stamp method". The representative transfer and output curves of the 2,6-DADTT-based SC-OFETs are respectively shown in Fig. 3g and h, with the highest mobility up to 1.26 cm^2 V^{-1} s^{-1} and the average mobility of 0.706 cm^2 V^{-1} s^{-1} (20 devices, Table S3 and Fig. S8†). The mobility distribution based on 20 devices is also shown in Fig. 3i. High current on/off ratio of $10^6 \sim 10^8$ are also achieved for the transistors. The hysteresis of the single crystal devices is very small and almost negligible (Fig. S9(a)–(e)†). At the same time, there is no significant change after multiple tests on the same device (Fig. S9(f)†). We also study the change in device performance with the variation of the single crystal thickness by characterizing three OFET devices with different crystal thickness (~30 nm, ~150 nm, ~400 nm), and the testing results showed that the mobility decreases sharply as the crystal thickness increases (Fig. S10†). The high mobility can be attributed to the densely herringbone packing, multiple intermolecular interactions, the highly ordered molecular packing and high quality of 2,6-DADTT single crystals.

In view of the high mobility and strong absorption in the UV region of 2,6-DADTT, the photo response behaviour was further studied. The diagrammatic sketch of 2,6-DADTT-based single crystal OPT is demonstrated in Fig. 4a. The representative I–V curves of the 2,6-DADTT-based OPT in dark and under various illumination intensities with fixed V_{DS} are shown in Fig. 4b. Under 365 nm illumination, the transfer curves of the OPTs show obvious positive V_T shift and increased I_{DS} as the illumination intensity increases. Photo-induced electron–hole pairs are generated under illumination and dissociated into carriers under vertical electric field. The holes easily flow to the drain electrode whereas the electrons accumulate at the source electrode. The accumulated electrons help to lower the injection barrier and decrease of the contact resistance, and lead to the shift of the threshold voltage and the increase of I_{DS}.[39] We also
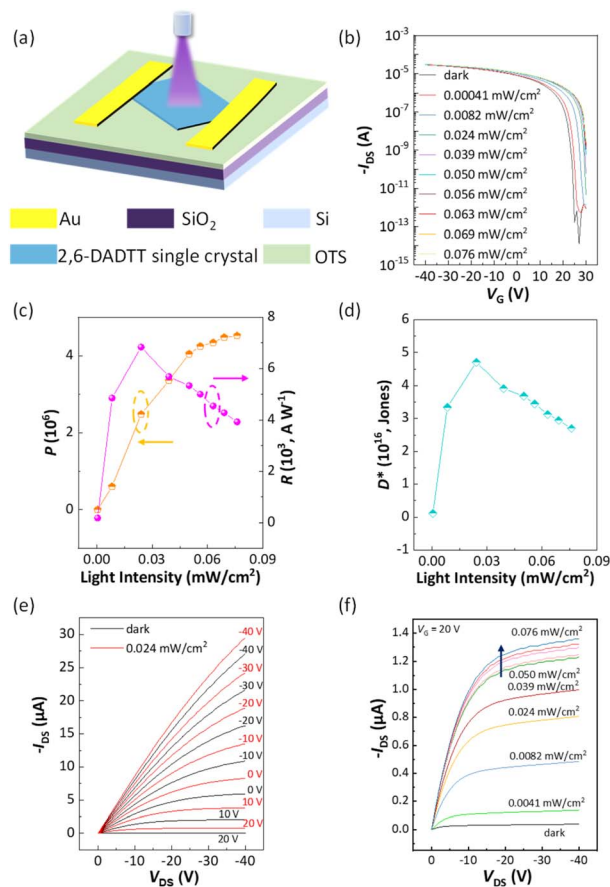

Fig. 4 (a) Diagrammatic sketch of 2,6-DADTT single crystal phototransistors. (b) The transfer curves of 2,6-DADTT-based single crystal phototransistors under various light intensity (365 nm) compared to that in darkness. (c) and (d) P, R and D^* variation under different light intensity. (e) Output characteristics with different V_G under UV light illumination (intensity: 0.024 mW cm^{-2}) and in dark. (f) $-I_{DS}$ under various light illumination intensities ($V_G = 20$ V).

noticed considerable V_T shift and increased I_{DS} even under very weak illumination intensity of 0.0082 mW cm^{-2}, suggesting its capability for weak UV light detection. Photosensitivity (P), photoresponsivity (R), and detectivity (D^*) are three key parameters to evaluate the performance of OPTs, which can be calculated according to eqn (S1)–(S3).† The 2,6-DADTT-based OPTs show excellent response behaviour to UV light (365 nm) with P, R, D^* respectively reaching 2.49×10^6, 6.84×10^3 A W^{-1}, and 4.70×10^{16} Jones at an illumination intensity of 0.024 mW cm^2. The P, R and D^* as a function of light intensity are shown in Fig. 4c and d. According to the calculation formula of P, it is only related to the photocurrent (I_{photo}) and dark current (I_{dark}), in which the I_{photo} increases with the increase of the incident light intensity (P_i), while the I_{dark} remains unchanged. Therefore, P value is positively correlated with the P_i, while R value is related not only to the I_{photo} and I_{dark}, but also to the P_i and the illuminated channel area (S). As the P_i gradually increases, the growth rate of I_{photo} become slow, after calculation, the result of R value will show a changing trend of first increasing and then decreasing as the light intensity increases, and a maximum value will appear. As for D^*, the parameters in the calculation formula of D^* are

constants except for R, so the changing trend of D^* is the same as R. To the best of our knowledge, the P, R and D^* are among the best values for UV-sensitive OPTs reported till now (Table S4†). Output characteristics with different V_G under UV light illumination (intensity: 0.024 mW cm^{-2}) or in dark were also characterized (Fig. 4e), showing obvious increase of the output current upon illumination. The I–V curves with incident light as the modulation gate were also exhibited in Fig. 4f, demonstrating that output current increase with the modulation of the light intensity. The temporal response of the 2,6-DADTT-based OPT was also tested (Fig. S11†), showing long-range plasticity (LTP) behaviour like artificial synapses under light stimulation, which will be further studied in the future. Besides, we also tested the stability of 2,6-DADTT single crystal phototransistor over 15 days. During this period, the values of P, R and D^* exhibited no significant changes (Fig. S12†), and as a result, the device shows excellent comprehensive performance as well as good stability.

Conclusions

In summary, a novel organic semiconductor, 2,6-DADTT, was designed and synthesized by introducing anthracene group at 2,6-positions of dithieno[3,2-b:2′,3′-d]thiophene. Single crystal structure of 2,6-DADTT presents classical herringbone packing and multiple intermolecular interactions, including S⋯S (3.470 Å), S⋯C (3.304 Å, 3.391 Å, 3.394 Å) and C–H⋯π (2.763 Å, 2.822 Å, 2.846 Å, 2.865 Å, 2.885 Å, 2.890 Å) contacts, were observed. 2,6-DADTT-based SC-OFETs reach a highest mobility of 1.26 cm^2 V^{-1} s^{-1} and an average mobility of 0.706 cm^2 V^{-1} s^{-1}. 2,6-DADTT-based single crystal OPTs demonstrate P value of 2.49 × 10^6, R value of 6.84 × 10^3 A W^{-1} and ultrahigh D^* value of 4.70 × 10^{16} Jones, which are among the best figures of merits for UV-sensitive OPTs. These excellent comprehensive performances indicate its well application prospect in integrated optoelectronics, especially in the field of UV light detection or other new emerging vision sensors.

Author contributions

Y. Lou conceived the idea, carried out the experiments and wrote the manuscript under the supervision of J. Li. L. Yu, H. Zhang, T. Jiang, and Y. Hu assisted in the measurements of the electrical characteristics. L. Zhang helped with characterizations of the single crystals. Y. Sun carried out theoretical calculations and gave valuable suggestions about the work. D. Ji, L. Li and W. Hu gave valuable suggestions about the manuscript writing. All authors have given approval to the final version of the manuscript.

Conflicts of interest

There are no conflicts to declare.

Acknowledgements

Notes and references

1 J. G. Mei, Y. Diao, A. L. Appleton, L. Fang and Z. N. Bao, *J. Am. Chem. Soc.*, 2013, **135**, 6724–6746.
2 C. L. Wang, H. L. Dong, W. P. Hu, Y. Q. Liu and D. B. Zhu, *Chem. Rev.*, 2012, **112**, 2208–2267.
3 Y. Z. Lin, Y. F. Lia and X. W. Zhan, *Chem. Soc. Rev.*, 2012, **41**, 4245–4272.
4 H. F. Ling, S. H. Liu, Z. J. Zheng and F. Yan, *Small Methods*, 2018, **2**, 1800070.
5 T. Someya, Z. N. Bao and G. G. Malliaras, *Nature*, 2016, **540**, 379–385.
6 Y. Zheng, Z. A. Yu, S. Zhang, X. Kong, W. Michaels, W. C. Wang, G. Chen, D. Y. Liu, J. C. Lai, N. Prine, W. M. Zhang, S. Nikzad, C. B. Cooper, D. L. Zhong, J. Mun, Z. T. Zhang, J. Kang, J. B.-H. Tok, L. McCulloch, J. Qin, X. D. Gu and Z. N. Bao, *Nat. Commun.*, 2021, **12**, 5701.
7 S. M. Duan, B. W. Geng, X. T. Zhang, X. C. Ren and W. P. Hu, *Matter*, 2021, **4**, 3415–3443.
8 X. Yu, C. Li, C. Y. Gao, X. S. Zhang, G. X. Zhang and D. Zhang, *SmartMat*, 2021, **2**, 347–366.
9 T. Higashihara, *Polym. J.*, 2021, **53**, 1061–1071.
10 S. M. Duan, X. Gao, Y. Wang, F. X. Yang, M. X. Chen, X. T. Zhang, X. C. Ren and W. P. Hu, *Adv. Mater.*, 2019, **31**, 1807975.
11 C. Wang, X. C. Ren, C. H. Xu, B. B. Fu, R. H. Wang, X. T. Zhang, R. J. Li, H. X. Li, H. L. Dong, Y. G. Zhen, S. B. Lei, L. Jiang and W. P. Hu, *Adv. Mater.*, 2018, **30**, 1706260.
12 H. Minemawari, T. Yamada, H. Matsui, J. Y. Tsutsumi, S. Haas, R. Chiba, R. Kumai and T. Hasegawa, *Nature*, 2011, **475**, 364–367.
13 H. Roh, C. Cunin, S. Samal and A. Gumyusenge, *MRS Commun.*, 2022, **12**, 565–577.
14 Z. T. Zhang, W. C. Wang, Y. W. Jiang, Y. X. Wang, Y. L. Wu, J. C. Lai, S. M. Niu, C. Y. Xu, C. Shih, C. Wang, H. P. Yan, L. Galuska, N. Prine, H. C. Wu, D. L. Zhong, G. Chen, N. Matsuhisa, Y. Zheng, Z. A. Yu, Y. Wang, R. Dauskardt, X. D. Gu, J. B.-H. Tok and Z. N. Bao, *Nature*, 2022, **603**, 624–643.
15 Y. Zhao, Y. L. Guo and Y. Q. Liu, *Adv. Mater.*, 2013, **25**, 5372–5391.
16 H. L. Dong, X. L. Fu, J. Liu, Z. R. Wang and W. P. Hu, *Adv. Mater.*, 2013, **25**, 6158–6183.
17 H. Sirringhaus, *Adv. Mater.*, 2014, **26**, 1319–1335.
18 B. S. Zhou, W. R. Liu, Y. C. Xu, C. X. Jin, J. L. Yang and J. Sun, *J. Phys. D: Appl. Phys.*, 2022, **55**, 304006.
19 J. P. Zeng, D. W. He, J. S. Qiao, Y. T. Li, L. Sun, W. S. Li, J. C. Xie, S. Gao, L. J. Pan, P. Wang, Y. Xu, Y. Li, H. Qiu, Y. Shi, J. B. Xu, W. Ji and X. R. Wang, *Nat. Commun.*, 2023, **14**, 324.
20 W. R. Liu, G. M. Zhang, C. X. Jin, Y. C. Xu, Y. L. Nie, X. F. Shi, J. Sun and J. L. Yang, *Appl. Phys. Lett.*, 2022, **121**, 073301.

21 L. Q. Liu, C. Cai, Z. J. Zhang, S. T. Zhang, J. Deng, B. Yang, C. Gu and Y. G. Ma, *ACS Mater. Lett.*, 2021, **3**, 428–432.

22 Y. J. Wan, J. Deng, W. L. Wu, J. D. Zhou, Q. Niu, H. Y. Li, H. K. Yu, C. Gu and Y. G. Ma, *ACS Appl. Mater. Interfaces*, 2020, **12**(39), 43976–43983.

23 J. Deng, Z. Zhang, P. Sang, S. Yin, S. Zhang, Y. Li, B. Yang, C. Gu and Y. Ma, *Aggregate*, 2023, e313, DOI: **10.1002/agt2.313**.

24 J. Li, K. Zhou, J. Liu, Y. G. Zhen, L. Liu, J. D. Zhang, H. L. Dong, X. T. Zhang, L. Jiang and W. P. Hu, *J. Am. Chem. Soc.*, 2017, **139**, 17261–17264.

25 Z. S. Qin, H. K. Gao, J. Y. Liu, K. Zhou, J. Li, Y. Y. Dang, L. Huang, H. X. Deng, X. T. Zhang, H. L. Dong and W. P. Hu, *Adv. Mater.*, 2019, **31**, 1903175.

26 Z. S. Qin, C. Gao, H. K. Ga, T. Y. Wang, H. L. Dong and W. P. Hu, *Sci. Adv.*, 2022, **8**, eabp8775.

27 J. Li, Z. S. Qin, Y. J. Sun, Y. G. Zhen, J. Liu, Y. Zou, C. L. Li, X. Y. Lu, L. Jiang, X. T. Zhang, D. Y. Ji, L. Q. Li, H. L. Dong and W. P. Hu, *Angew. Chem., Int. Ed.*, 2022, **61**, e202206825.

28 Y. W. Xu, P. Xu, D. H. Hu and Y. G. Ma, *Chem. Soc. Rev.*, 2021, **50**, 1030–1069.

29 M. R. Zhu and C. L. Yang, *Chem. Soc. Rev.*, 2013, **42**, 4963–4976.

30 X. Tang, L. S. Cui, H. C. Li, A. J. Gillett, F. Auras, Y. K. Qu, C. Zhong, S. T. E. Jones, Z. Q. Jiang, R. H. Friend and L. S. Liao, *Nat. Mater.*, 2020, **19**, 1332–1338.

31 J. Y. Wang and X. W. Zhan, *Acc. Chem. Res.*, 2021, **54**, 132–143.

32 Y. H. Liu, B. W. Liu, C. Q. Ma, F. Huang, G. T. Feng, H. Z. Chen, J. H. Hou, L. P. Yan, Q. Y. Wei, Q. Luo, Q. Y. Bao, W. Ma, W. Liu, W. W. Li, X. J. Wan, X. T. Hu, Y. C. Han, Y. W. Li, Y. H. Zhou, Y. P. Zou, Y. W. Chen, Y. F. Li, Y. S. Chen, Z. Tang, Z. C. Hu, Z. G. Zhang and Z. S. Bo, *Sci. China Chem.*, 2022, **65**, 224–268.

33 H. F. Yao, L. Ye, H. Zhang, S. S. Li, S. Q. Zhang and J. H. Hou, *Chem. Rev.*, 2016, **116**, 7397–7457.

34 Y. L. Guo, G. Yu and Y. Q. Liu, *Adv. Mater.*, 2010, **22**, 4427–4447.

35 X. H. Huang, D. Y. Ji, H. Fuchs, W. P. Hu and T. Li, *ChemPhotoChem*, 2020, **4**, 9–38.

36 D. Y. Ji, T. Li, J. Liu, S. Amirjalayer, M. Z. Zhong, Z. Y. Zhang, X. H. Huang, Z. M. Wei, H. L. Dong, W. P. Hu and H. Fuchs, *Nat. Commun.*, 2019, **10**, 12.

37 C. Wang, X. T. Zhang and W. P. Hu, *Chem. Soc. Rev.*, 2020, **49**, 653–670.

38 Q. Tang, G. P. Zhang, B. Jiang, D. Ji, H. H. Kong, K. Riehemann, Q. M. Ji and H. Fuchs, *SmartMat*, 2021, **2**, 109–118.

39 K. J. Baeg, M. Binda, D. Natali, M. Caironi and Y. Y. Noh, *Adv. Mater.*, 2013, **25**, 4267–4295.

40 Q. Y. Li, Y. L. Guo and Y. Q. Liu, *Chem. Mater.*, 2019, **31**, 6359–6379.

41 C. Wang, X. C. Ren, C. H. Xu, B. B. Fu, R. H. Wang, X. T. Zhang, R. J. Li, H. X. Li, H. L. Dong, Y. G. Zhen, S. B. Lei, L. Jiang and W. P. Hu, *Adv. Mater.*, 2018, **30**, 1706260.

42 G. Y. Zhao, J. Liu, Q. Meng, D. Y. Ji, X. T. Zhang, Y. Zou, Y. G. Zhen, H. L. Dong and W. P. Hu, *Adv. Electron. Mater.*, 2015, **1**, 1500071.

43 A. Y. Li, L. J. Yan, M. Liu, I. Murtaza, C. He, D. W. Zhang, Y. W. Hea and H. Meng, *J. Mater. Chem. C*, 2017, **5**, 5304–5309.

44 J. W. Tao, D. Liu, Z. S. Qin, B. Shao, J. B. Jing, H. X. Li, H. L. Dong, B. Xu and W. J. Tian, *Adv. Mater.*, 2020, **32**, 1907791.

45 X. X. Yu, L. Zheng, J. F. Li, P. P. Yu, Z. Y. Liu, C. G. Li, Y. Zou, X. T. Zhang and W. P. Hu, *Org. Electron.*, 2020, **87**, 105941.

46 Y. S. Guan, J. Qiao, Y. Y. Liang, H. K. Bisoyi, C. Wang, W. Xu, D. B. Zhu and Q. Li, *Light: Sci. Appl.*, 2022, **11**, 236.

47 L. Zhang, L. Tan, Z. H. Wang, W. P. Hu and D. B. Zhu, *Chem. Mater.*, 2009, **21**, 1993–1999.

48 A. L. Briseno, Q. Miao, M. M. Ling, C. Reese, H. Meng, Z. N. Bao and F. Wudl, *J. Am. Chem. Soc.*, 2006, **128**, 15576–15577.